Molecular Cancer Therapeutics

Small Molecule Inhibition of MDM2–p53 Interaction Augments Radiation Response in Human Tumors

Lauryn R. Werner[1], Shyhmin Huang[1], David M. Francis[1], Eric A. Armstrong[1], Fang Ma[1], Chunrong Li[1], Gopal Iyer[1], Jude Canon[2], and Paul M. Harari[1]

Abstract

MDM2–p53 interaction and downstream signaling affect cellular response to DNA damage. AMG 232 is a potent small molecule inhibitor that blocks the interaction of MDM2 and p53. We examined the capacity of AMG 232 to augment radiation response across a spectrum of human tumor cell lines and xenografts. AMG 232 effectively inhibited proliferation and enhanced radiosensitivity via inhibition of damage repair signaling. Combined AMG 232 and radiation treatment resulted in the accumulation of γH2AX-related DNA damage and induction of senescence with promotion of apoptotic and/or autophagic cell death. Several molecules involved in senescence, autophagy, and apoptosis were specifically modulated following the combined AMG 232/radiation treatment, including FoxM1, ULK-1, DRAM, and BAX. *In vivo* xenograft studies confirmed more potent antitumor and antiangiogenesis efficacy with combined AMG 232/radiation treatment than treatment with drug or radiation alone. Taken together, these data identify the capacity of AMG 232 to augment radiation response across a variety of tumor types harboring functional p53. *Mol Cancer Ther; 14(9); 1994–2003. ©2015 AACR.*

Introduction

The p53 tumor suppressor is a key modulator of tumorigenesis and a central target in cancer therapy (1). Commonly referred to as a master regulator, p53 has the ability to initiate a variety of cellular responses upon activation, including cell cycle arrest, senescence, apoptosis, and autophagy (2). In cancers retaining wild-type (wt) *p53*, protein function is limited by MDM2, the primary negative regulator of p53. Inhibition of p53 by MDM2 is achieved via suppression of transcriptional activity, promotion of cytoplasmic export, and/or protein degradation (3).

Given the pivotal role of p53 in tumor suppression, several therapeutic strategies to activate p53 by disrupting the negative control by MDM2 have been investigated. Many approaches have been described, including antisense oligonucleotides against MDM2, small molecule inhibitors of MDM2 ubiquitin ligase activity, and small molecule MDM2 inhibitors, which hinder p53–MDM2 interaction (4). In 2004, the identification of Nutlin-3 as the first small molecule inhibitor of MDM2 spurred interest in this approach, which led to the development of several analogous compounds (5). Recent studies have demonstrated the antitumor capacity of small molecule MDM2 inhibitors both *in vitro* and *in vivo*, and several of these compounds have advanced to clinical trials (1, 6).

AMG 232 is an inhibitor of MDM2 that is designed to target the p53-binding site of MDM2, which covers amino acids 17 to 111 in the N-terminus (refs. 7, 8; Supplementary Fig. S1A). AMG 232 robustly activates p53 signaling and has potent antitumor activity in both *in vitro* and *in vivo* models (7, 9). Emerging evidence has linked MDM2 to the radiation-induced DNA damage repair response by a direct binding to Nbs1 that is a critical member of the Mre11-Nbs1-Rad50 repair pathway (10).

Radiation is a core cancer treatment modality delivered to over 50% of all cancer patients during the course of their disease. Although very effective when high dose can be delivered, radiation is frequently limited by normal tissue tolerance. There is a compelling rationale to identify promising molecular targeting agents that may sensitize tumor cells to radiation (11). Considering the significant role of both p53 and MDM2 in the regulation of radiation response, and the activation of p53 achieved by small molecule MDM2 inhibitors, the combination of AMG 232 and radiation may offer a valuable therapeutic approach in cancer therapy. In the current study, we evaluated the capacity of AMG 232 to augment radiation response across a variety of tumor types. In addition, we highlight the potential underlying molecular mechanisms involved in the regulation of AMG 232–mediated radiation response.

Materials and Methods

Reagents and antibodies

AMG 232 was provided by Amgen, Inc. Antibodies against MDM2, p53, p21, and Ki67 were obtained from Santa Cruz Biotechnology Inc.. Antibody against von Willebrand Factor was obtained from DakoCytomation, and anti–α-tubulin was

[1]Department of Human Oncology, University of Wisconsin School of Medicine and Public Health, Madison, Wisconsin. [2]Oncology Research Amgen, Inc., Thousand Oaks, California.

Note: Supplementary data for this article are available at Molecular Cancer Therapeutics Online (http://mct.aacrjournals.org/).

L.R. Werner and S. Huang contributed equally to this article.

Corresponding Author: Paul M. Harari, University of Wisconsin, K4/336, 600 Highland Avenue, Madison, WI 53792. Phone: 608-263-5009; Fax: 608-262-6256; E-mail: harari@humonc.wisc.edu

doi: 10.1158/1535-7163.MCT-14-1056-T

obtained from Calbiochem. All other antibodies were obtained from Cell Signaling Technology, and all other chemicals were purchased from Sigma. Cell culture media and supplements were obtained from Life Technologies, Inc.

Cell lines

Human lung H226 cell line was provided by Drs. John Minna and Adi Gazdar (University of Texas Southwestern Medical School, Dallas, TX), and remaining cell lines were obtained from ATCC, including H460 (lung), A549 (lung), H1299 (lung), HCT116 (colorectal), A375 (melanoma), SJSA-1 (sarcoma), and MCF-7 (breast). The authenticity of these cell lines was verified on the basis of cell morphology and genomic short tandem repeat (STR) profile of each cell line 4 to 6 months before commencing the current study.

Ionizing radiation, clonogenic survival, and cell viability assay

Cells were irradiated with a ^{137}Cs-irradiater (Shepherd & Associates). For clonogenic survival assays, cells irradiated with various doses were seeded in 6-well plates. Following 10 to 14 days, colonies were stained with crystal violet and colonies consisting of 50 cells or more were scored. The surviving fraction was determined as the total number of colonies formed divided by the total number of cells seeded. Radiation survival curves were plotted after normalization for the cytotoxicity induced by control or drug alone. Cell viability was examined either by crystal violet staining or propidium iodide (PI) dye exclusion flow cytometric assay as described previously (12). Following staining with PI (30 μg/mL) for 30 minutes, dead cells permeable to PI were quantified by analyzing the geometric mean fluorescence intensity (GMFI) of PI in 10,000 cells.

Quantification of mRNA expression

Relative mRNA levels of *p53*, *p21*, *MDM2*, *FOXM1*, *ULK1*, *DRAM1*, and *BAX* were quantified via real-time PCR (RT-qPCR) using a Bio-Rad iQ5 RT-qPCR Detection System and Power SYBR Green PCR Master Mix (Life Technologies). All reactions were performed in triplicate. The geometric mean of three reference genes (*GAPDH*, *PGK*, and *TBP*) was calculated and used as an endogenous control. Fold changes after treatments were normalized to a control sample at time 0. Detailed primer information for each molecule is provided in the "Supplementary Materials and Methods."

Flow cytometric analysis of γH2AX

Following treatments, cells were fixed in ice-cold 70% ethanol followed by rehydration for 10 minutes at 4°C in PBS containing 1% BSA and 0.2% Triton X-100. Cells were then stained with anti–phosho-Histone H2AX (γH2AX) (Ser139) mAb (Clone JBW301; EMD Millipore) overnight at 4°C followed by an AF488-secondary antibody for 1 hour. Following centrifugation, cells were resuspended in PI solution to determine the cell cycle phase for cells with γH2AX as described previously (13).

Senescence-associated β-galactosidase detection

Cells (2×10^4) were plated in 6-well plates and treated with AMG 232 and/or radiation. Following 72 hours of treatment, cells were stained for senescence-associated β-galactosidase using the Senescence Detection kit (Cell Signaling Technology).

Immunofluorescence

Cells in chamber slides were fixed in 4% paraformaldehyde and permeabilized with 0.2% Triton X-100. Cells were then probed with anti-FoxM1 Ab, followed by AF488-secondary Ab. The number of nuclear FoxM1-positive cells was analyzed using Image J software.

Detection of acidic vesicular organelles with acridine orange staining

Acidic vesicular organelles (AVO), as marker of autophagy, were detected by acridine orange (AO) flow cytometry as described previously (14). To quantify the development of AVOs, cells were stained with 1 μg/mL of AO for 15 minutes and were then removed from the plate with trypsin-EDTA and collected for flow cytometric analysis.

Apoptosis and mitochondria membrane potential

Apoptosis was detected by flow cytometry using an Annexin V/PI dual staining kit from BD Biosciences Pharmingen as described previously (15). Mitochondrial membrane potential was examined using JC-1 dye as described previously (16). In healthy cells, the polarized mitochondrial membrane potential ($\Delta\psi$) drives JC-1 uptake into the mitochondria, where JC-1 aggregates form and fluoresce red. The loss of mitochondrial membrane potential was determined by a decreased radio of red to green fluorescence.

Tumor xenograft studies

Athymic nude mice were obtained from Harlan Bioproducts for Science, and the care of experimental animals was conducted in accordance with institutional guidelines. Tumor cells were injected subcutaneously into the dorsal flank of the mice. Tumor volume was monitored by direct measurement with calipers and calculated by the formula: $\pi/6 \times$ (large diameter) $\times$ (small diameter)^2. AMG 232 was administered daily via oral gavage at the specified doses and time intervals. Radiation treatment was delivered with a cabinet X-ray biologic irradiator X-RAD 320 from Precision X-Ray, Inc. For A375 xenograft, the A375 SQ2 cell line was used to achieve more uniform and reproducible tumor growth. A375 SQ2 was generated by performing two serial *in vivo* passages of A375 cells as described previously (17).

Statistical analysis

Prism 5 (GraphPad Software) was used for all statistical analyses. For clonogenic assays, the Bonferroni Multiple Comparison Test was applied. For all other experiments, the Student *t* test was used. In all results, unless otherwise indicated, the data reflect at least 2 independent experiments and were reported as mean ± SD. For all graphs, *, $P < 0.05$; **, $P < 0.01$; and ***, $P < 0.001$.

Results

AMG 232 activates p53 signaling and inhibits tumor cell proliferation

To assess the effect of AMG 232 on p53 signaling, we measured p53, MDM2, and p21 protein levels across a panel of tumor cell lines, including lung (A549, H460, H226, and H1299), melanoma (A375), breast (MCF7), colon (HCT116), and osteosarcoma (SJSA-1). All cell lines harbor wt *p53* except

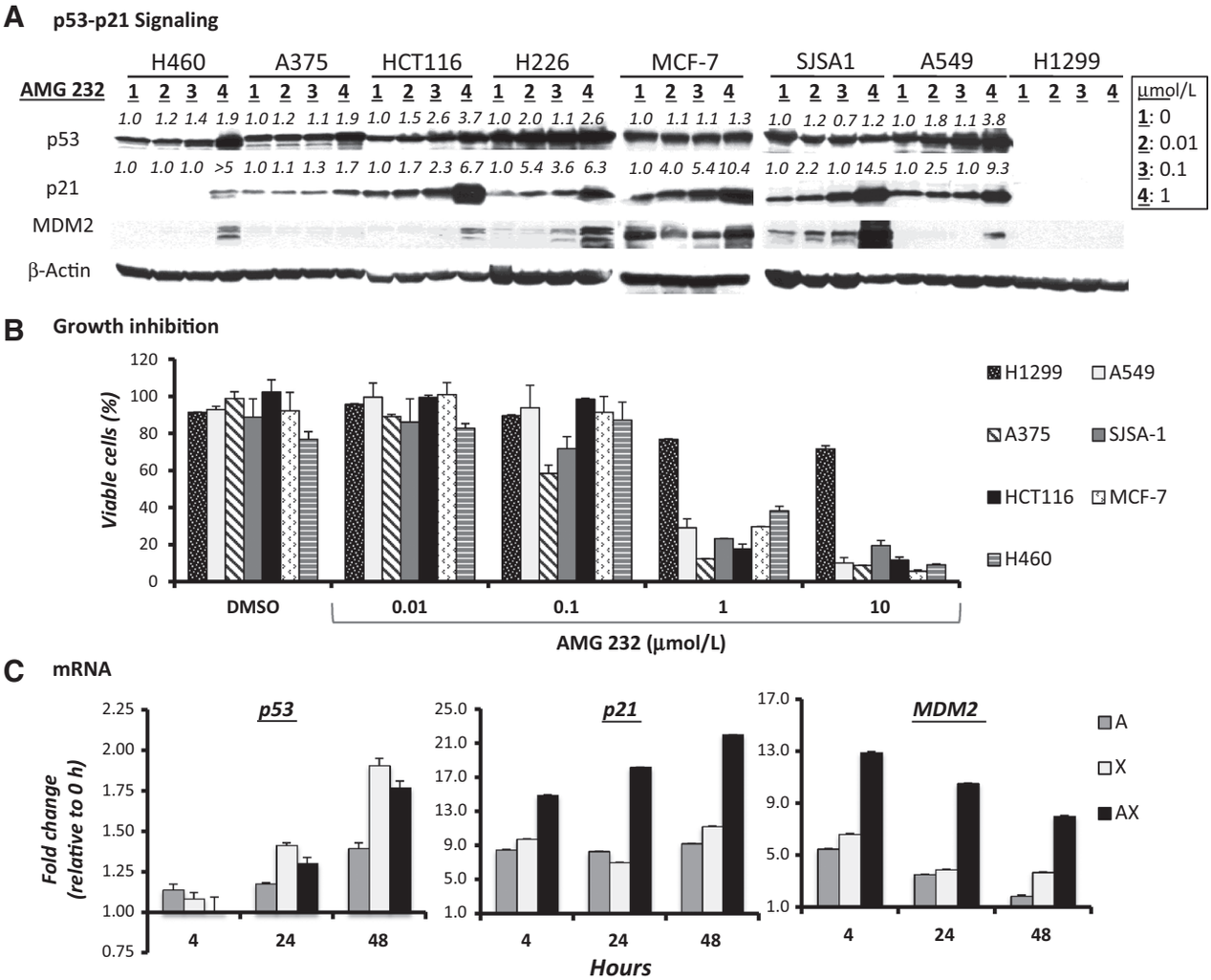

Figure 1.
Effect of AMG 232 on p53 activation and cell proliferation. A, representative immunoblot images depict dose-dependent activation of p53-p21 signaling following AMG 232 treatment for 24 hours. Protein levels in each blot were quantified using ImageJ, and the fold increase in p53 and p21 was determined following normalizing to the β-actin loading control and the untreated control sample in each cell line. B, cells were exposed to 0 to 10 µmol/L of AMG 232 for 3 to 5 days. Viable cells were then determined using crystal violet staining as described in Materials and Methods. DMSO represents vehicle control at 10 µmol/L of AMG 232. C, A375 cells were treated with AMG 232 (A, 0.5 µmol/L) and/or radiation (X, 2 Gy) for 0 to 48 hours. Relative expression of *p53*, *p21*, and *MDM2* mRNA compared with the control at 0 hour was determined by RT-qPCR as described in "Materials and Methods."

H1299, which is *p53* null. AMG 232 activated p53-p21 signaling in a dose-dependent manner in the majority of cell lines tested (Fig. 1A). Similar to previous studies, the degree of p53 induction varied among different cell lines, likely reflecting differences in the baseline level of p53 and MDM2 as well as the optimal dose/time response to AMG 232 (9). However, a consistent and profound induction of p21 level was observed in all cell lines tested. Because p21 is the key indicator of p53 activity, this observation confirms the ability of AMG 232 to activate p53. AMG 232 also promoted an increase in MDM2, resulting from negative feedback autoregulation induced by p53 activation. Importantly, the impact of AMG 232 to activate p53-p21 signaling translates well into a profound antiproliferative effect. AMG 232 significantly reduced cell proliferation in a dose-dependent manner in all *p53* wt cell lines tested, as shown in Fig. 1B.

To further confirm activation of p53 and explore the potential interaction between AMG 232 and radiation, we examined the effect of AMG 232 and/or radiation on mRNA expression of *p53* and targeted genes *p21* and *MDM2*. A375 cells were presented, because melanoma is a compelling candidate for AMG 232 due to its high rate of wt p53. In accordance with the increase of protein level, we observed elevated expression of *p53*, *MDM2*, and *p21* genes following AMG 232 treatment at all time points tested (Fig. 1C). Similarly, radiation treatment resulted in increased expression of all three genes. However, the combined treatment of AMG 232 and radiation induced a more profound increase in *p21* and *MDM2* expression than single modality

treatment, suggesting that the combination was more potent in activating the p53 pathway. Similar results were observed in SJSA-1 (Supplementary Fig. S1B). Cell cycle analysis revealed that treatment with AMG 232 and radiation resulted in a significant cell cycle arrest in both G_1 and G_2–M phases (Supplementary Fig. S1C), consistent with upregulation of the cell cycle inhibitor p21. Taken together, these results suggest an interaction between AMG 232 and radiation reflecting an upregulation of p53-p21 signaling.

AMG 232 enhances radiosensitivity of tumor cells

We investigated the effect of AMG 232 on radiosensitivity using clonogenic survival analysis. As shown in Fig. 2A, the addition of AMG 232 to radiation treatment significantly reduced clonogenic survival in all cell lines except *p53*-null H1299 cells. A mechanistic study revealed that the combination of AMG 232 and radiation significantly inhibited the activation and/or expression of several key proteins involved in DNA damage repair signaling (Supplementary Fig. S2A). We further examined the profile of DNA damage at different time points and cell cycle phases via flow cytometric analysis of γH2AX, a marker of DNA double-strand breaks (DSB). As shown in the 2-dimentional plots of Fig. 2B, radiation alone (C) induced a dramatic increase of γH2AX-positive cells, especially in late S and G_2–M phases (dotted box in the figure), that peaked 1 hour following treatment and subsequently declined (Fig. 2B, gray bar graph). However, in cells exposed to the combined treatment of AMG 232 and radiation (A), the percentage of γH2AX-positive cells re-elevated significantly at 24 and 48 hours. Similar results were observed in other

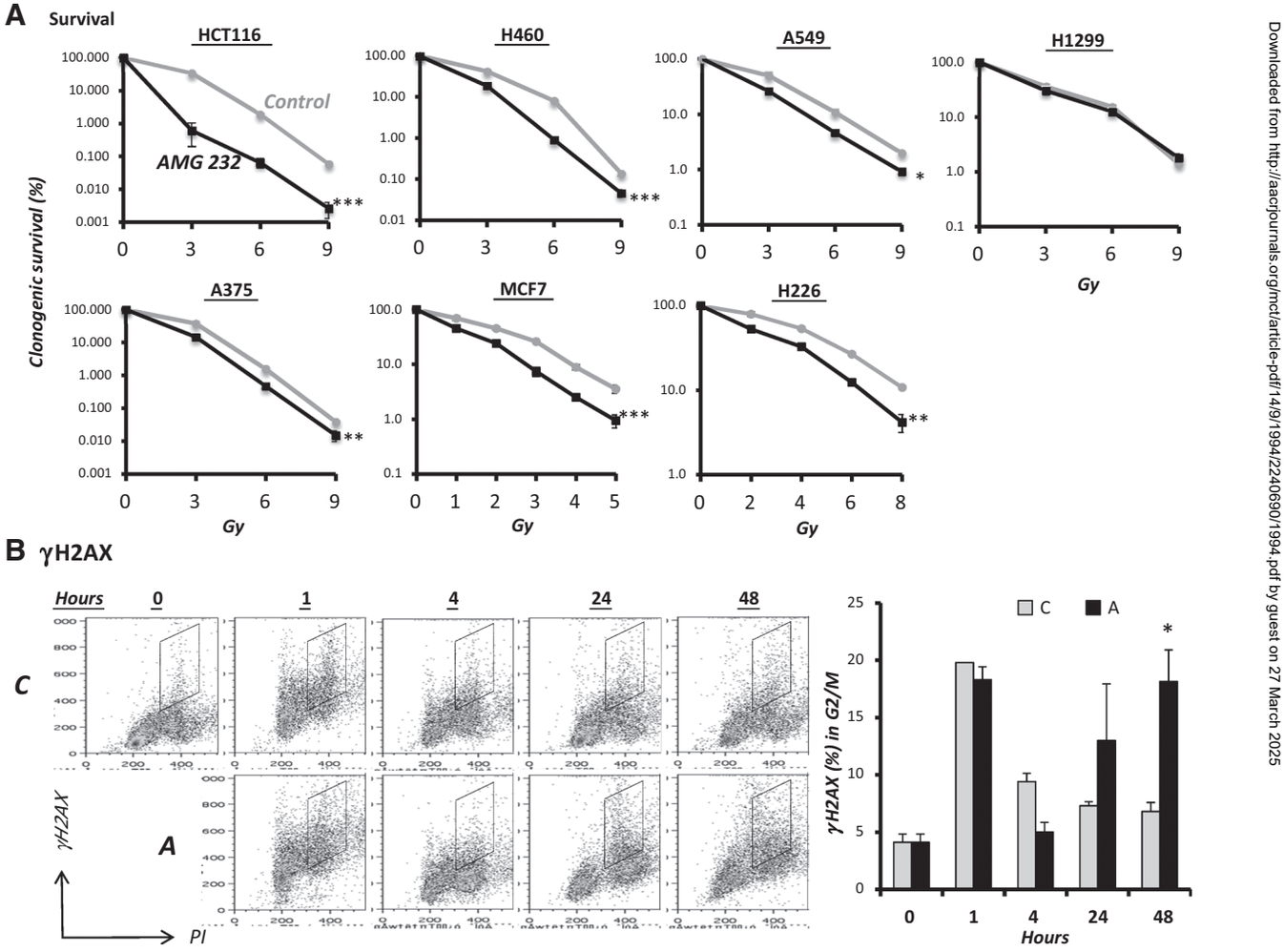

Figure 2.
Effect of AMG 232 on radiosensitivity. A, radiosensitivity of vehicle control (gray)- or AMG 232–treated (black) cells was examined by clonogenic survival analysis. Selected numbers of cells were treated with AMG 232 (HCT116, 1 μmol/L; H226, 0.4 μmol/L; all others, 0.5 μmol/L) or DMSO control followed by radiation. Results were expressed as the percentage of colony formation relative to cells without radiation in each group. B, radiation-induced DNA damage throughout the cell cycle was determined via flow cytometry, using anti-γH2AX antibody and PI staining as described in Materials and Methods. The left plot depicts bivariant cytogram of γH2AX level and DNA content in A375 cells obtained 0 to 48 hours after 2 Gy radiation in the presence of DMSO (C, top) or AMG 232 (A, bottom) treatment. The populations of γH2AX-labeled cells in G_2–M stage were gated (dotted box) in each cytogram and quantitated in the right bar graph. *, $P < 0.05$; **, $P < 0.01$; and ***, $P < 0.001$.

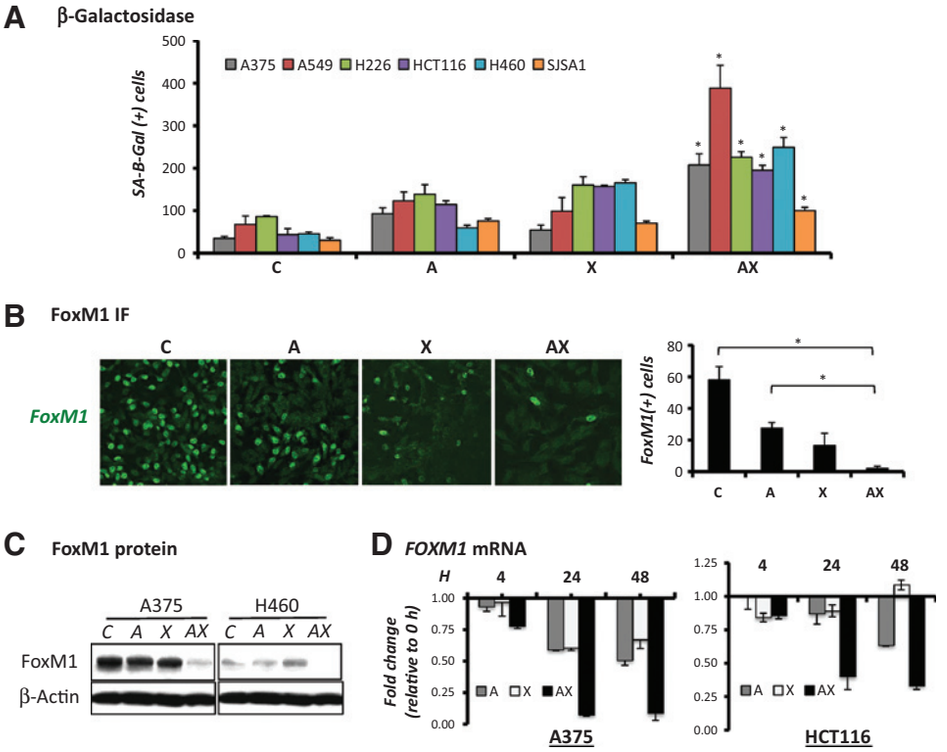

Figure 3.
Induction of cellular senescence by AMG 232 and radiation. A, cells were treated with vehicle control (C), AMG 232 (A, 0.5 μmol/L), radiation (X, 2 Gy), or both (AX) for 72 hours and subsequently stained for SA-β-Gal. The bar graph depicts the average number of SA-β-Gal–positive cells from three randomly selected images with equal cell confluency. B, immunofluorescence (IF) staining of FoxM1 at 48 hours following treatments. The right bar graph depicts the average number of FoxM1-positive cells determined from 3 randomly selected images. C and D, significant decrease of FoxM1 protein and mRNA levels at 24 and 48 hours following AMG 232 and/or radiation treatment.
*, $P < 0.05$.

cell lines, including H460, MCF7, A549, and H226 (Supplementary Fig. S2B and S2C). Notably, AMG 232 alone did not induce accumulation of γH2AX at 48 hours (Supplementary Fig. S2B). Because a lethally irradiated cell with unrepaired DSB may continue to divide and result in the reproduction of γH2AX in daughter cells, our findings suggest that AMG 232 enhances radiosensitivity by inhibiting DSB repair, resulting in the accumulation of dying cells with unrepaired lethal DNA damage.

AMG 232 in combination with radiation induces cellular senescence

Because γH2AX is also associated with senescence by binding to dysfunctional telomeres at the end of double strands (18), we investigated the effect of AMG 232 and radiation on cell senescence by examining several senescence markers. We first examined the activity of senescence-associated β-galactosidase (SA-β-Gal) and found that combined treatment of AMG 232 and radiation resulted in a significant increase in SA-β-gal–positive cells compared with treatment with either radiation or AMG 232 alone in all cell lines tested (Fig. 3A). Representative images of SA-β-gal staining for all cell lines tested are shown in Supplementary Fig. S3. Additional markers of senescence were examined to validate these findings.

FoxM1 is a critical proproliferative transcription factor, and its inhibition leads to cellular senescence (19). Immunofluorescent imaging in A375 cells revealed that treatment with either AMG 232 or radiation alone at 48 hours resulted in a minor reduction in nuclear FoxM1 staining, whereas combination treatment resulted in a significant reduction in the number of FoxM1-positive cells (Fig. 3B). Furthermore, immunoblotting and RT-PCR analysis confirmed a reduction in protein and mRNA levels of FoxM1 following the combined treatment of AMG 232 and radiation in A375 (Fig. 3B and C). Similar results were observed in H460 and HCT116 cells. These results suggest that AMG 232 radiosensitizes tumor cells in part by enhancing radiation-induced cellular senescence.

AMG 232 in combination with radiation induces autophagy

An interesting link between p53-mediated senescence and autophagy has been identified. A subset of autophagy-related genes are upregulated during senescence and apoptosis, including *ULK1* (unc-51 like autophagy activating kinase1) and *DRAM1* (damage-regulated autophagy modulator; refs. 20, 21). Combined treatment with AMG 232 and radiation resulted in a synergistic increase of *ULK1* and *DRAM1* mRNA at 24- to 48-hour time points, though AMG 232 alone induced a different response profile between these 2 genes (Fig. 4A). Similar results were observed in SJSA-1 cells (Supplementary Fig. S4A). To confirm AMG 232/radiation-induced autophagy, we examined the induction of autophagy-related AVOs (22) by AO staining. AO emits red fluorescence when it enters AVOs, but stains bright green in DNA and the cytoplasm. Treatment with either AMG 232 or radiation alone produced no significant increase in cells with AVOs, as shown in the upper two quadrants (FL3-AO-red) of the 2-dimentional plots, when compared with control (Fig. 4B). Strikingly, when cells were exposed to both AMG 232 and radiation, a robust increase of cells with AVOs was observed in all 4 cell lines tested. In H460 cells, an increase greater than 5-fold was observed (Fig. 4B, bar graph). In accordance with the increased gene expression of autophagy-related *ULK1* and *DRAM1*, our results suggest that autophagy is involved in AMG 232–regulated radiation response.

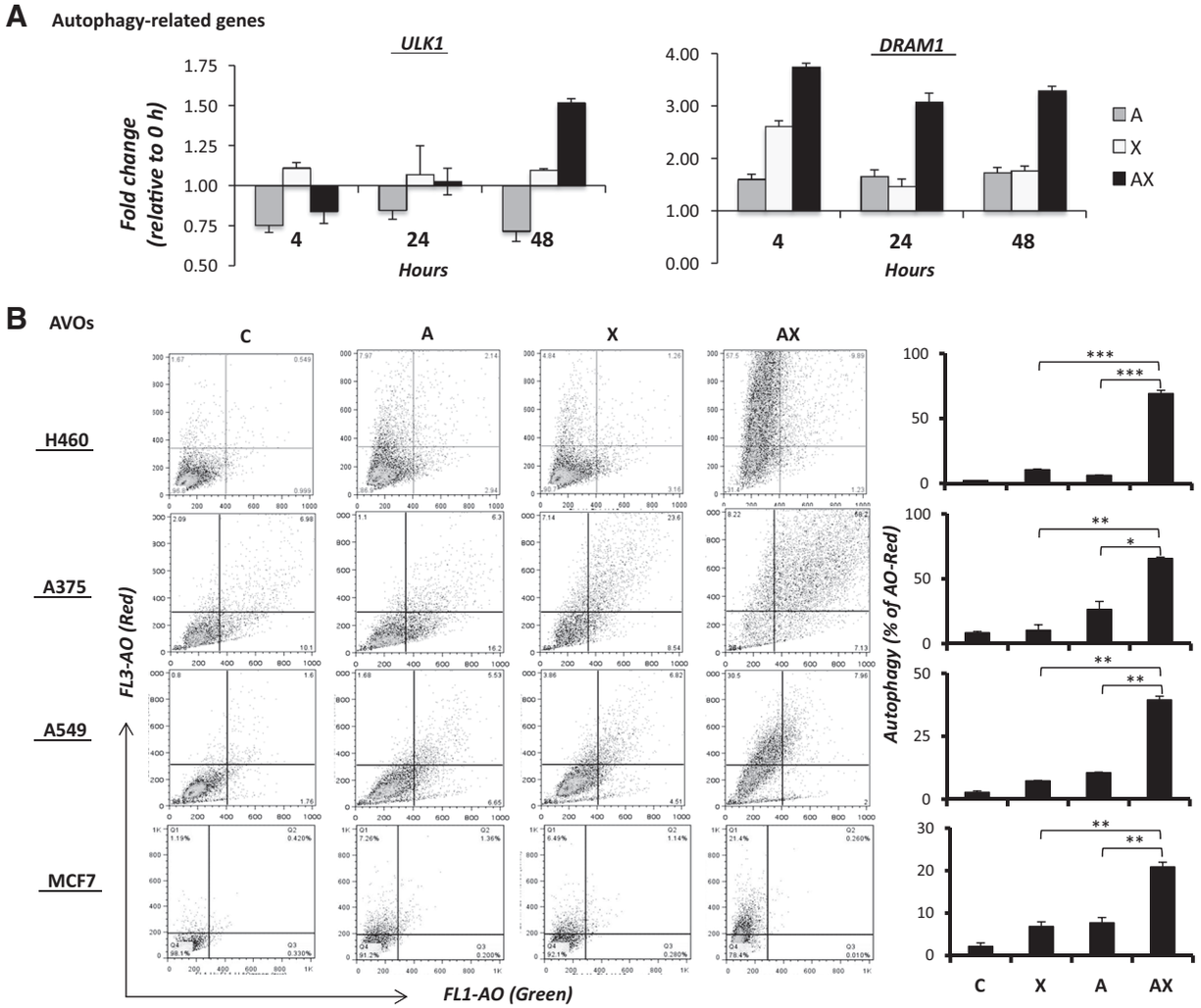

Figure 4.
Induction of autophagy by AMG 232 and radiation. A, A375 cells were treated with AMG 232 (A, 0.5 μmol/L) and/or radiation (X, 2 Gy) for 0 to 48 hours. Relative mRNA levels were then determined by RT-qPCR, normalizing to control at 0 hour. B, quantification of autophagy-related AVOs by AO flow cytometry as described in Materials and Methods. Cells were treated with either vehicle control (C), AMG 232 (A, 0.5 μmol/L), radiation (X, 2 Gy), or both (AX) for 72 hours followed by AO staining. The left plots depict representative cytograms of 4 cell lines from at least 3 independent experiments, and the right plot demonstrates the percentage of AO-positive cells with increased red fluorescence. *, $P < 0.05$; **, $P < 0.01$; and ***, $P < 0.001$.

AMG 232 in combination with radiation induces programmed cell death

Although autophagy is often induced under nutrient-limiting conditions as a mechanism for maintaining cell viability, progressive autophagy can be cytotoxic and substitute for apoptosis in the induction of cell death (23, 24). We first investigated whether the combined treatment of AMG 232 and radiation could induce programmed cell death by determining plasma membrane rupture in tumor cells. Treatment with AMG 232 or radiation alone resulted in a minimal accumulation of dead cells (Fig. 5A). However, combination treatment increased the proportion of dead cells with increased PI permeability in all cell lines tested. Furthermore, in cells subjected to combination treatment, a significant loss of mitochondrial membrane potential was detected by the uptake of lipophilic fluorochrome JC-1(12, 16). As shown in Fig. 5B, a significant reduction of JC-1 uptake, as indicated a reduced red/green fluorescence ratio, was observed in the combined treatment when compared with single treatments alone, indicating disruption of mitochondrial membrane integrity.

Because a loss of mitochondrial function is implicated in apoptosis (25), we further assessed the induction of apoptosis by Annexin V/PI flow cytometry analysis, which identifies cells in early (Annexin V–positive/PI negative) or late (double positive) phases of apoptosis. As shown in Fig. 5C, a 2- to 5-fold increase in the proportion of early apoptotic cells was observed 72 hours after AMG 232 or radiation treatment alone, whereas combination treatment resulted in a profound 12-fold increase. Similarly, combination treatment demonstrated an increase in the population of late apoptotic cells

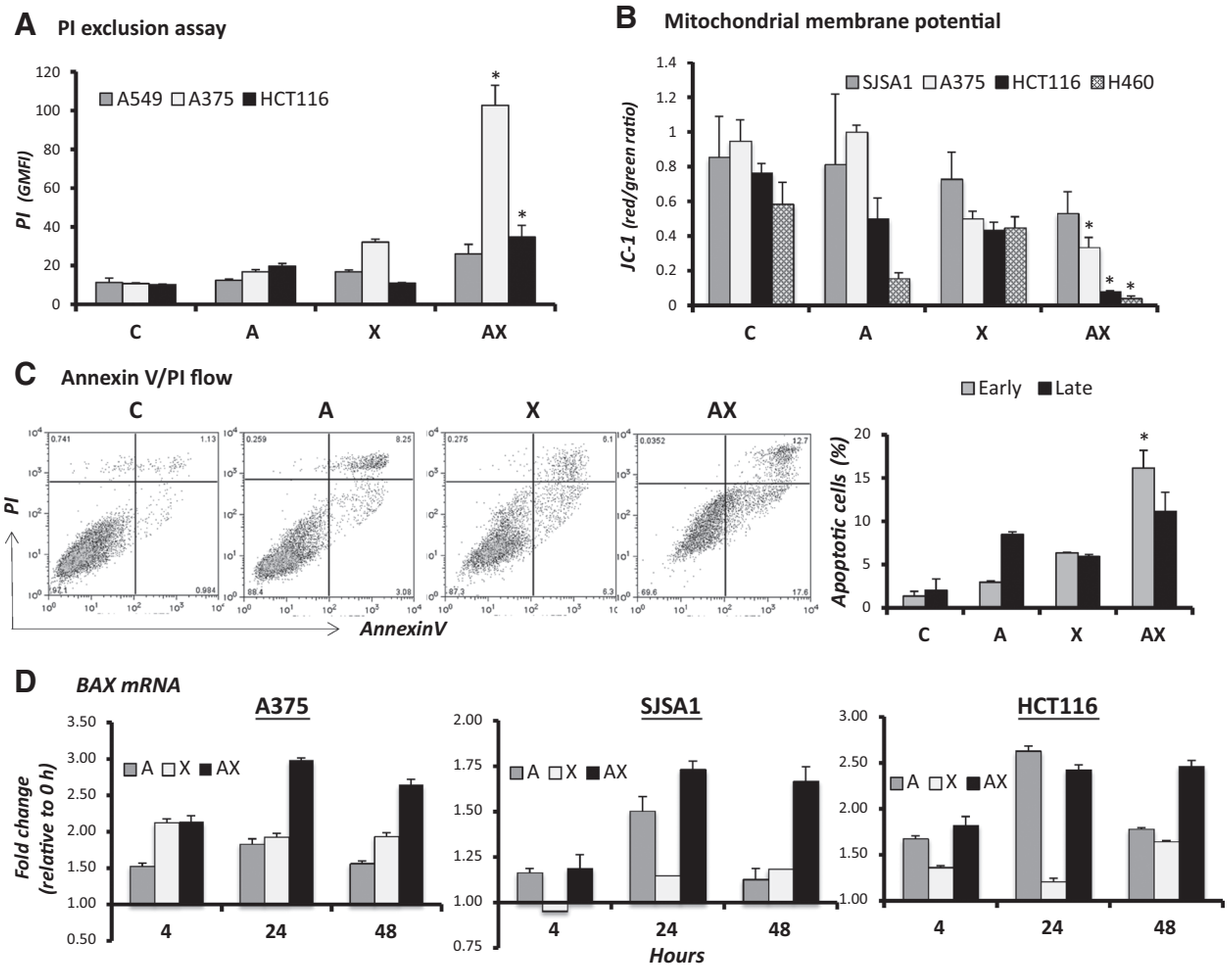

Figure 5.
Increase of programmed cell death by AMG 232 and radiation. A, rupture of plasma membrane was identified by PI exclusion assay. Cells were treated with either vehicle control (C), AMG 232 (A, 0.5 μmol/L), radiation (X, 6 Gy), or both (AX) for 72 hours. Values indicate the GMFI of PI. B, loss of mitochondrial membrane potential was identified by JC-1 assay as described in Materials and Methods. Values indicate the ratio of JC-1 aggregates (red) to JC-1 monomers (green). C, induction of apoptosis in A375 was identified by Annexin V/PI apoptosis analysis. The graphical representation of the percentages of early and late apoptotic cells was derived from representative cytograms. D, proapoptotic *Bax* expression following 0 to 48 hours of AMG 232 (A), radiation (X), or combined treatment (AX). *, $P < 0.05$.

superior to that of either treatment alone. In accordance with these results, we also found a significant increase in gene expression of proapoptotic *BAX* 24 to 48 hours after combined treatment with AMG 232 and radiation in both A375 and SJSA-1 cells (Fig. 5D). Taken together, these results suggest that the addition of AMG 232 to radiation treatment caused the induction of cellular senescence and autophagy, which ultimately resulted in cell death.

AMG 232 augments radiation response in human tumor xenografts

We next investigated the capacity of AMG 232 to augment radiation response in a variety of human tumor xenografts, representing different genetic backgrounds and tissue types, including lung carcinoma, melanoma, sarcoma, and colorectal carcinoma. In order to best capture the interaction between AMG 232 and radiation, doses and schedules of both treatment modalities were selected from previous studies (7, 9) for each cell line such that single-agent impact on tumor growth inhibition would be modest, in the range of 10% to 30%. Remarkably, in every xenograft model, the combination of AMG 232 and radiation led to superior antitumor efficacy compared with single modality treatment as shown in Fig. 6. After cessation of treatment, tumors in the combination treatment groups remained cytostatic and failed to regrow, suggesting a senescence phenotype consistent with our previous *in vitro* observations. Notably, there was no significant difference in the body weight profile of mice receiving combined treatment when compared with that in radiation- or AMG 232–treated mice across our xenograft experiments (Supplementary Fig. S5). AMG 232 appears to be well tolerated at dose levels tested when combined with radiation in these animal experiments.

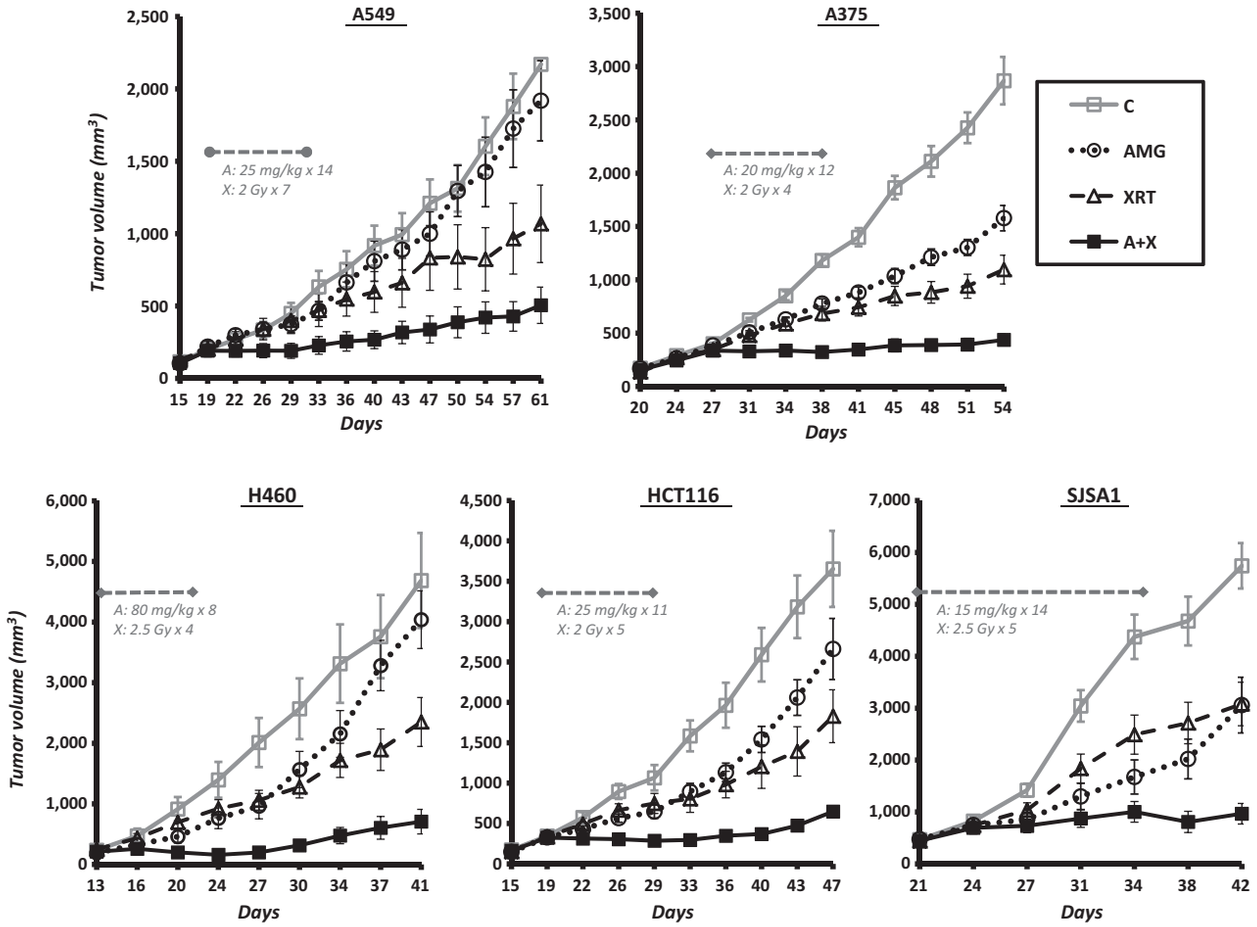

Figure 6.
AMG 232 augments radiation response in human tumor xenografts. Mice with tumor xenografts of 5 cell lines were treated with vehicle control (C), AMG 232 (AMG), radiation (XRT), or both modalities (A+X) during the time interval indicated by the dotted gray line in each figure (n = 6–10 mice per group).

To validate the functional observation in xenografts, we further examined the histology of H460 & SJSA-1 tumor specimens by IHC. By detecting a cellular proliferation marker Ki67, we found that the number of proliferating cells was significantly decreased in both H460 and SJSA-1 tumors receiving combined treatment of AMG 232 and radiation when compared with tumors receiving single modality treatment (Supplementary Fig. S6A). These findings confirm and strengthen the antitumor capacity of AMG 232 when combined with radiation. In concordance with reduced tumor volumes, we also found a significant reduction of vascular density in both H460 and SJSA-1 tumors receiving combined treatment of AMG 232 and radiation by staining with an endothelial cell marker, von Willebrand factor (vWF; Supplementary Fig. S6B). Taken together, these results suggest that AMG 232 may augment radiation response by inhibiting tumor cell proliferation and by interfering with tumor-associated angiogenesis.

Discussion

MDM2 inhibitors are a class of p53-activating agents that may be of considerable value in cancer therapeutics. Because impaired p53 function is associated with a reduced sensitivity of tumor cells to radiation, there has been considerable interest to activate p53 to promote enhanced efficacy of radiotherapy. In the current study, we present a potent MDM2 inhibitor, AMG 232, that effectively inhibits tumor proliferation and augments radiation response across a wide variety of solid tumor types expressing wt *p53*. Exposure of cancer cells to AMG 232 leads to activation of p53-p21 signaling and gene expression (Fig. 1). More importantly, we identify that the combination of AMG 232 and radiation induces a synergistic effect on p53-regulated downstream cellular events involved in the response to radiation-induced DNA damage. In particular, a profound augmentation of senescence and autophagy is observed in cells following combined treatment with AMG 232 and radiation.

Premature cellular senescence has been shown to be a principal mode of cell death accounting for radiation response in cancer cells retaining p53 function (26, 27). Therapy-induced senescence is now recognized for its contribution to the overall loss of tumor cell viability (28). By examining several senescence markers, we consistently found a significant induction of senescence following combined AMG 232 and radiation

treatment. This was identified by an increase in senescence-associated β-galactosidase and p21 as well as a decrease in FoxM1 expression (Figs. 3 and 1). Interestingly, AMG 232/radiation treatment also resulted in a robust increase of γ-H2AX in G_2–M phase cells 48 hours after the initial burst observed 1 hour following treatment. In contrast, treatment with radiation or AMG 232 alone did not produce a significant impact on γ-H2AX accumulation at 48 hours (Fig. 2B). Because previous studies have revealed γ-H2AX as a potential senescence marker (18), the retention of γ-H2AX in G_2–M-arrested cells at the later time points suggests the presence of DNA lesions with unrepairable DSBs in senescent cells. Consequently, a significant increase in cell death was observed in cells subjected to combination treatment, as indicated by either loss of mitochondrial function or rupture of cell membrane (Fig. 5). Our results further support previous findings that reveal the retention of residual γ-H2AX, not the early γ-H2AX peak, as an indication of lethal DNA damage that induces a reduction in clonogenic survival (29, 30).

Another interesting finding of this study is the involvement of autophagy in AMG 232–regulated radiation response. As shown in Fig. 4, a profound increase of autophagy-related AVOs was identified in cells following combined treatment with AMG 232 and radiation. Furthermore, autophagy-related *ULK-1* and *DRAM* genes were significantly upregulated in cells treated with AMG 232 and radiation. Although autophagy is often considered to be a cell survival mechanism, there is also evidence for the capacity of autophagy to mediate the antiproliferative and/or cytotoxic actions of selected anticancer agents (31, 32). Furthermore, a direct crosstalk between apoptosis and autophagy has been identified that serves to reinforce cell death (33). In the context of p53 activation, Broz and colleagues highlighted an intimate connection between p53 and autophagy that contributes to efficient p53-dependent apoptosis and cancer suppression (34). Nevertheless, the precise factors that determine whether p53-induced programmed cell death occurs through apoptosis or autophagy remain elusive. In some cell lines examined in our current study, such as H460 and A549, we found that autophagy was conducive to cell death when induction of apoptosis was weak or absent (Supplementary Fig. S4B). However, A375 cells exhibited both autophagy and apoptosis following combined treatment with AMG 232 and radiation. Additional experiments are under way to explore the molecular mechanisms and genetic backgrounds of various cell lines that may account for differential induction of programmed cell death following AMG 232 and radiation treatment.

The markedly increased antitumor capacity of AMG 232 and radiation observed in xenograft studies suggest that factors involved in the tumor–stromal interaction, such as angiogenesis, may influence radiation response *in vivo*. We found that vascular density was significantly reduced in tumors receiving combined treatment of AMG 232 and radiation (Supplementary Fig. S6). Although AMG 232 exhibits a 40-fold lower affinity for mouse MDM2 than for human MDM2 in biochemical studies, the decrease of vasculature observed in tumor xenografts likely reflects the decreased tumor growth and tumor-release of angiogenic factors, such as VEGF. MDM2 has shown to be a positive activator of VEGF, and MDM2 inhibitors block VEGF-mediated tumor angiogenesis (35). Our findings reveal the potential antiangiogenic capacity of AMG 232 that may contribute to the augmentation of radiation response observed in xenograft studies. A detailed investigation is under way to examine temporal changes of the tumor microenvironment following AMG 232 treatment, including hypoxia and vascular normalization, representing two important factors involved in regulating tumor response to radiation (36, 37).

Previous studies have shown a p53-independent impact of MDM2 inhibitors in tumor cells without functional p53. Using *p53*-null HCT116 (−/−) and PC3 cells, Lau and colleagues found that treatment with Nutlin-3 at 10 to 40 μmol/L suppressed cell growth and increased apoptosis by inhibiting the interaction of MDM2 and p73, a p53 isoform (38). Later, a p53-independent role of Nutlin-3 in radiation-induced DNA damage response was also reported (39, 40). Although AMG 232 did not inhibit proliferation of H1299 at 10 μmol/L as shown in Fig. 1A, we found that AMG 232 could effectively inhibit tumor growth at a concentrations above 10 μmol/L in cells without wt *p53*, including H1299, SCC1, and SCC1483 (Supplementary Fig. S7A). Interestingly, the p53-independent antiproliferation effect of AMG 232 seemingly had no reliance on MAPK and AKT proliferation/survival signaling, but rather, on cell cycle progression pathway via Rb and FoxM1 as shown in Supplementary Fig. S7B. FoxM1 is of great interest, as it was also significantly reduced following combined AMG 232/radiation treatment in cells with functional p53 (Fig. 3). Moreover, it has been shown recently that suppression of FoxM1 sensitized cancer cells to apoptosis induced by DNA damage (41). Because FoxM1 transcriptionally activates genes involved in cell cycle progression and radiation-induced DNA damage repair (42, 43), we are currently examining the underlying mechanism of FoxM1 in regulating AMG 232–induced p53-dependent and p53-independent radiation response. Although the p53-independent impact of MDM2 inhibitors is intriguing, this may reflect off target effects and the clinical relevance and safety profile of high-dose AMG 232 or Nutlin-3 would require detailed evaluation.

In summary, AMG 232 demonstrates the capacity to augment radiation response across a variety of human tumors, including lung, breast, colorectal, melanoma, and sarcoma. Using multiple approaches and multiple cell lines, we confirm the augmentation of radiation response by AMG 232 resulting from induction of cellular senescence and programmed cell death. For tumors with wt *p53*, and potentially in select tumors without functional p53, AMG 232 may afford broad future application in cancer therapy in combination with radiation. The strong interaction of AMG 232 with radiation appears worthy of systematic clinical trial investigation. Several phase I/II clinical trials are currently in progress to evaluate the clinical potential of AMG 232 in advanced solid tumors (refs. 1, 6; *ClinicalTrials.gov*).

Disclosure of Potential Conflicts of Interest

No potential conflicts of interest were disclosed.

Authors' Contributions

Conception and design: L.R. Werner, S. Huang, G. Iyer, J. Canon, P.M. Harari
Development of methodology: L.R. Werner, S. Huang, D.M. Francis, E.A. Armstrong, G. Iyer, J. Canon, P.M. Harari

Acquisition of data (provided animals, acquired and managed patients, provided facilities, etc.): L.R. Werner, S. Huang, D.M. Francis, E.A. Armstrong, F. Ma
Analysis and interpretation of data (e.g., statistical analysis, biostatistics, computational analysis): L.R. Werner, S. Huang, F. Ma, G. Iyer, J. Canon, P.M. Harari
Writing, review, and/or revision of the manuscript: L.R. Werner, S. Huang, D.M. Francis, C. Li, G. Iyer, J. Canon, P.M. Harari
Administrative, technical, or material support (i.e., reporting or organizing data, constructing databases): L.R. Werner, S. Huang, D.M. Francis, P.M. Harari
Study supervision: L.R. Werner, S. Huang, D.M. Francis, G. Iyer, P.M. Harari

Grant Support

This work was supported in part by laboratory research funding from Amgen, Inc. (to P.M. Harari).

The costs of publication of this article were defrayed in part by the payment of page charges. This article must therefore be hereby marked *advertisement* in accordance with 18 U.S.C. Section 1734 solely to indicate this fact.

Received December 12, 2014; revised June 17, 2015; accepted June 27, 2015; published OnlineFirst July 10, 2015.

References

1. Khoo KH, Verma CS, Lane DP. Drugging the p53 pathway: understanding the route to clinical efficacy. Nat Rev Drug Discov 2014;13:217–36.
2. Sullivan KD, Gallant-Behm CL, Henry RE, Fraikin J-L, Espinosa JnM. The p53 circuit board. BBA-Rev Cancer 2012;1825:229–44.
3. Fahraeus R, Olivares-Illana V. Mdm2's social network. Oncogene 2014;33:4365–76.
4. Selivanova G. Wild type p53 reactivation: from lab bench to clinic. FEBS Lett 2014;588:2628–38.
5. Klein C, Vassilev LT. Targeting the p53-mdm2 interaction to treat cancer. Br J Cancer 2004;91:1415–9.
6. Zhao Y, Aguilar A, Bernard D, Wang S. Small-molecule inhibitors of the mdm2-p53 protein-protein interaction (mdm2 inhibitors) in clinical trials for cancer treatment. J Med Chem 2015;58:1038–52.
7. Sun D, Li Z, Rew Y, Gribble M, Bartberger MD, Beck HP, et al. Discovery of amg 232, a potent, selective, and orally bioavailable mdm2-p53 inhibitor in clinical development. J Med Chem 2014;57:1454–72.
8. Rew Y, Sun D. Discovery of a small molecule mdm2 inhibitor (amg 232) for treating cancer. J Med Chem 2014;57:6332–41.
9. Canon J, Osgood T, Olson SH, Saiki AY, Robertson R, Yu D, et al. The mdm2 inhibitor amg 232 demonstrates robust antitumor efficacy and potentiates the activity of p53-inducing cytotoxic agents. Mol Cancer Ther 2015;14:649–58.
10. Alt JR, Bouska A, Fernandez MR, Cerny RL, Xiao H, Eischen CM. Mdm2 binds to nbs1 at sites of DNA damage and regulates double strand break repair. J Biol Chem 2005;280:18771–81.
11. Lin SH, George TJ, Ben-Josef E, Bradley J, Choe KS, Edelman MJ, et al. Opportunities and challenges in the era of molecularly targeted agents and radiation therapy. J Natl Cancer Inst 2013;105:686–93.
12. Brenner JC, Graham MP, Kumar B, Saunders LM, Kupfer R, Lyons RH, et al. Genotyping of 73 um-scc head and neck squamous cell carcinoma cell lines. Head Neck 2010;32:417–26.
13. Huang X, Darzynkiewicz Z. Cytometric assessment of histone h2ax phosphorylation: a reporter of DNA damage. Methods Mol Biol 2006; 314:73–80.
14. Zhu X, Wu L, Qiao H, Han T, Chen S, Liu X, et al. Autophagy stimulates apoptosis in her2-overexpressing breast cancers treated by lapatinib. J Cell Biochem 2013;114:2643–53.
15. Benavente S, Huang S, Armstrong EA, Chi A, Hsu K-T, Wheeler DL, et al. Establishment and characterization of a model of acquired resistance to epidermal growth factor receptor targeting agents in human cancer cells. Clin Cancer Res 2009;15:1585–92.
16. Perelman A, Wachtel C, Cohen M, Haupt S, Shapiro H, Tzur A. Jc-1: alternative excitation wavelengths facilitate mitochondrial membrane potential cytometry. Cell Death Dis 2012;3:e430.
17. Carnahan J, Beltran PJ, Babij C, Le Q, Rose MJ, Vonderfecht S, et al. Selective and potent raf inhibitors paradoxically stimulate normal cell proliferation and tumor growth. Mol Cancer Ther 2010;9:2399–410.
18. Sedelnikova OA, Horikawa I, Zimonjic DB, Popescu NC, Bonner WM, Barrett JC. Senescing human cells and ageing mice accumulate DNA lesions with unrepairable double-strand breaks. Nat Cell Biol 2004;6:168–70.
19. Barsotti AM, Prives C. Pro-proliferative foxm1 is a target of p53-mediated repression. Oncogene 2009;28:4295–305.
20. Wong PM, Puente C, Ganley IG, Jiang X. The ulk1 complex: sensing nutrient signals for autophagy activation. Autophagy 2013;9:124–37.
21. Crighton D, Wilkinson S, O'Prey J, Syed N, Smith P, Harrison PR, et al. Dram, a p53-induced modulator of autophagy, is critical for apoptosis. Cell 2006;126:121–34.
22. Chen Y, Azad MB, Gibson SB. Methods for detecting autophagy and determining autophagy-induced cell death. Can J Physiol Pharmacol 2010;88:285–95.
23. White E, DiPaola RS. The double-edged sword of autophagy modulation in cancer. Clin Cancer Res 2009;15:5308–16.
24. Eisenberg-Lerner A, Kimchi A. The paradox of autophagy and its implication in cancer etiology and therapy. Apoptosis 2009;14:376–91.
25. Salido M, Gonzalez JL, Vilches J. Loss of mitochondrial membrane potential is inhibited by bombesin in etoposide-induced apoptosis in pc-3 prostate carcinoma cells. Mol Cancer Ther 2007;6:1292–9.
26. Lehmann BD, McCubrey JA, Jefferson HS, Paine MS, Chappell WH, Terrian DM. A dominant role for p53-dependent cellular senescence in radiosensitization of human prostate cancer cells. Cell Cycle 2007;6:595–605.
27. Luo H, Yount C, Lang H, Yang A, Riemer EC, Lyons K, et al. Activation of p53 with nutlin-3a radiosensitizes lung cancer cells via enhancing radiation-induced premature senescence. Lung Cancer 2013;81:167–73.
28. Ewald JA, Desotelle JA, Wilding G, Jarrard DF. Therapy-induced senescence in cancer. J Natl Cancer Inst 2010;102:1536–46.
29. Olive PL. Retention of gammah2ax foci as an indication of lethal DNA damage. Radiother Oncol 2011;101:18–23.
30. Banath JP, Klokov D, MacPhail SH, Banuelos CA, Olive PL. Residual gammah2ax foci as an indication of lethal DNA lesions. BMC Cancer 2010;10:4.
31. Notte A, Leclere L, Michiels C. Autophagy as a mediator of chemotherapy-induced cell death in cancer. Biochem Pharmacol 2011;82:427–34.
32. Macintosh RL, Ryan KM. Autophagy in tumour cell death. Semin Cancer Biol 2013;23:344–51.
33. Giansanti V, Torriglia A, Scovassi AI. Conversation between apoptosis and autophagy: "Is it your turn or mine?". Apoptosis 2011;16:321–33.
34. Kenzelmann Broz D, Spano Mello S, Bieging KT, Jiang D, Dusek RL, Brady CA, et al. Global genomic profiling reveals an extensive p53-regulated autophagy program contributing to key p53 responses. Genes Dev 2013;27:1016–31.
35. Xiong J, Yang Q, Li J, Zhou S. Effects of mdm2 inhibitors on vascular endothelial growth factor-mediated tumor angiogenesis in human breast cancer. Angiogenesis 2014;17:37–50.
36. Dewhirst MW, Cao Y, Moeller B. Cycling hypoxia and free radicals regulate angiogenesis and radiotherapy response. Nat Rev Cancer 2008;8:425–37.
37. Kleibeuker EA, Griffioen AW, Verheul HM, Slotman BJ, Thijssen VL. Combining angiogenesis inhibition and radiotherapy: a double-edged sword. Drug Resist Updat 2012;15:173–82.
38. Sharma P, Allison JP. The future of immune checkpoint therapy. Science 2015;348:56–61.
39. Valentine JM, Kumar S, Moumen A. A p53-independent role for the mdm2 antagonist nutlin-3 in DNA damage response initiation. BMC Cancer 2011;11:79.
40. Supiot S, Hill RP, Bristow RG. Nutlin-3 radiosensitizes hypoxic prostate cancer cells independent of p53. Mol Cancer Ther 2008;7:993–9.
41. Halasi M, Gartel AL. Suppression of foxm1 sensitizes human cancer cells to cell death induced by DNA-damage. PLoS ONE 2012;7:e31761.
42. Wang Z, Zheng Y, Park HJ, Li J, Carr JR, Chen YJ, et al. Targeting foxm1 effectively retards p53-null lymphoma and sarcoma. Mol Cancer Ther 2013;12:759–67.
43. Wonsey DR, Follettie MT. Loss of the forkhead transcription factor foxm1 causes centrosome amplification and mitotic catastrophe. Cancer Res 2005;65:5181–9.